

THE PRESENT WORK WAS SUBMITTED TO THE DEPARTMENT OF CONTINUUM  
MECHANICS

RHEINISCH-WESTFÄLISCHE TECHNISCHE HOCHSCHULE AACHEN  
FACULTY OF MECHANICAL ENGINEERING

## MASTER THESIS

# NONLINEAR MATERIAL PARAMETER IDENTIFICATION OF SOFT MATERIALS BASED ON AN INVERSE FINITE ELEMENT METHOD APPROACH

Presented by:	Nadia Pinedo Oruna, B.Sc.
Study programme:	General Mechanical Engineering M.Sc.
Matriculation number:	397 011
Reviewer:	Univ.-Prof. Dr.-Ing. Mikhail Itskov
Supervisor:	Rasul Abdulsalamov, M.Sc.
External supervisor:	Prof. Kazumi Matsui



## Declaration of Authorship

I declare that this work has been composed by myself, and describes my own work, unless otherwise acknowledged in the text.

All sentences or passages quoted in this paper from other people's work have been specifically acknowledged by clear cross-referencing to author, work and page(s). Any photos and illustrations which are not the work of the author have been used with the explicit permission of the originator and are specifically acknowledged.

This work has not been and will not be submitted for any other degree or the obtaining of ECTS points at the RWTH Aachen University or any other institution of higher education.

Aachen, 25<sup>th</sup> of May 2023

---

Nadia Pinedo Oruna, B.Sc.



# Contents

<b>1</b>	<b>Introduction</b>	<b>1</b>
1.1	Background and Problem Statement . . . . .	1
1.2	Objective and Scope of the Study . . . . .	1
1.3	State of the Art . . . . .	2
1.3.1	Experimental Characterization for Soft Materials . . . . .	2
1.3.2	Material Modeling of Soft Materials . . . . .	4
1.3.3	Inverse Finite Element Method for Parameter Identification . . . . .	4
1.3.4	Standard Verification and Validation for Computational Solid Mechanics (ASME) . . . . .	6
1.4	Overview . . . . .	6
<b>2</b>	<b>Experimental Model</b>	<b>7</b>
2.1	Experimental Model I . . . . .	8
2.2	Experimental Model II . . . . .	10
2.3	Experimental Tests Description . . . . .	12
2.3.1	Middle Point . . . . .	12
2.3.2	Load-Unloading . . . . .	13
2.3.3	Nearby Point . . . . .	14
2.4	Analysis and Overview of the Data and Results . . . . .	14
2.4.1	Middle Point . . . . .	15
2.4.2	Load-Unloading . . . . .	17
2.4.3	Nearby Point . . . . .	19
2.5	Main Assumptions for Material Modeling . . . . .	20
2.5.1	Level 1: Linear elasticity . . . . .	21
2.5.2	Level 2: Hyperelasticity . . . . .	22
<b>3</b>	<b>Computational model</b>	<b>23</b>
3.1	Middle point . . . . .	23
3.1.1	Description . . . . .	23
3.1.2	Analysis and Complications . . . . .	23
3.1.3	Verification of the Simulation Model . . . . .	23
3.2	Nearby point . . . . .	23
<b>4</b>	<b>Inverse Finite Element Method for Material Parameter Identification</b>	<b>25</b>
4.1	Procedure of IFEM . . . . .	25
4.2	Material Modeling . . . . .	25
4.2.1	Response Surface Optimization . . . . .	25
4.2.2	Objective Function Optimization . . . . .	25
4.2.3	Analysis and Comparison of Each Approach . . . . .	25

<b>5 Results</b>	<b>27</b>
5.1 Overview and Analysis . . . . .	27
5.2 Framework proposal . . . . .	27
5.3 Verification and Validation . . . . .	27
5.3.1 Deeper indentation . . . . .	27
5.3.2 Deformation profile analysis . . . . .	27
5.4 Limitations and implications of the results . . . . .	27
5.4.1 First Experimental model . . . . .	27
5.4.2 Second Experimental model . . . . .	28
5.5 Material model framework assumptions . . . . .	28
5.5.1 First Material model . . . . .	29
Linear elasticity . . . . .	29
Hyperelasticity . . . . .	29
5.6 Computational model . . . . .	29
5.7 Material model . . . . .	29
<b>6 Conclusion and Outlook</b>	<b>31</b>
6.1 Summary and Contributions . . . . .	31
6.2 Recommendations for Future Research . . . . .	31
6.3 Conclusions and Final Remarks . . . . .	31
<b>A Frequently Asked Questions</b>	<b>33</b>
A.1 How do I change the colors of links? . . . . .	33
<b>Bibliography</b>	<b>35</b>

# List of Figures

1.1	Nanoindentation . . . . .	4
2.1	First experimental model: Tensile and compression machine with an indenter with a rounded head. Test Specimen made from ultra-soft polyurethane resin positioned on a fixed platform with a similar shape for constraint. . . . .	8
2.2	First experimental model: Specimen dimensions made from ultra-soft polyurethane resin for indentation test. . . . .	9
2.3	YNU experimental model: 6-axis sensor Test Specimen made from ultra-soft polyurethane resin positioned on a fixed platform with a similar shape for constraint. . . . .	11
2.4	YNU experimental model: Loading diagram showing initial position of the indenter in normal position [11]. . . . .	11
2.5	Middle test point: Loading point on the top surface of the specimen. .	12
2.6	Load-Unload Case: Experimental model I with modified configuration setup, on top of the movable crosshead a displacement transducer was equipped to capture unloading data. . . . .	13
2.7	Nearby test point: Loading points for each experimental model to analyze shear stresses and to vbe employed for the validation of the computation models. . . . .	14
2.8	Load-displacement curve experimental data for Middle Point use case for both experimental models. . . . .	16
2.9	Total Force Reaction-Displacement curve: Comparison between experimental data for Middle Point use case from both models. . . . .	16
2.10	Load-displacement curve experimental data for Load-Unload use case for both experimental models. . . . .	17
2.11	Load-Unload Use Case: Analysis of Viscoelastic material properties by using six different indentation speeds. Load-Displacement curves were obtained from the first experimental test configuration. . . . .	18
2.12	Total Force Reaction-Displacement curve: Comparison between experimental data for Middle Point and Nearby Point. This point was located 5 mm right from the midpoint, following the minor axis of the ellipsoid. . . . .	19
2.13	Nearby Point Use Case: Analysis of shear stresses by observing three different nearby points on the specimens surface. Load-Displacement curves were gathered from Experimental Model II showing each force component. . . . .	20
5.1	Expdata . . . . .	28



# List of Tables



# List of Abbreviations

<b>FEA</b>	Finite Element Analysis
<b>FEM</b>	Finite Element Method
<b>iFEM</b>	inverse Finite Element Method
<b>ASME</b>	(The) American Society (of) Mechanical Engineering



# Physical Constants

Speed of Light  $c_0 = 2.997\,924\,58 \times 10^8 \text{ m s}^{-1}$  (exact)



# List of Symbols

$a$	distance	m
$P$	power	$\text{W} (\text{J s}^{-1})$
$\omega$	angular frequency	rad



# 1 Introduction

## 1.1 Background and Problem Statement

The biomechanical characterization of soft tissues has gained attention in medical research, in areas such as medical image analysis and visualization. For many years, the obtained medical diagnoses were often based on the assumptions of experts or their accumulated experience. While this information have proven to be useful in general, these methods have limitations in cases where quantifiable data is necessary, specifically for computer-assisted systems, e.g., medical diagnosis, therapy, and training [8]. To gather the material data, e.g., elasticity, stiffness, response under deformation and temperature, it is required to gain access to the soft tissues and perform in-vivo testing experiments. However, obtaining accurate biomechanical data can be challenging due to the invasive nature of the procedures and the difficulty in maintaining constant and reproducible internal or external factors in experimental configurations.

Especially, when it comes to internal organs, obtaining reliable data for examination after their extraction is difficult because the material properties can vary between samples or testing locations on the same organ. This is due to the influence of various factors such as changes in blood pressure, changes in material properties over time, symptoms of disease, and more. In addition, another problem is the lack of replication, due to the use of different individuals' organs, which introduces more external factors into the equation. Moreover, given a tissue sample, it is difficult to properly characterize the material due to its anisotropic property, which can lead potentially to inaccuracies in the result.

In the situation where the material data can be collected in a constant, fast and reliable process, a material model can be established and the computer-aided systems can predict the mechanical behavior of soft tissues, providing preoperative calculations. This demonstrates the importance of material data collection and material model development, especially in the context of computational models such as engineering simulation models created finite element analysis (FEA) software and their medical applications in medical devices, surgical procedures, and training softwares. By using accurate material models, the accuracy of the simulation can be improved, aiding in a better understanding and predicting a soft tissue response to external stimuli, making them more useful in medical research and other related applications.

## 1.2 Objective and Scope of the Study

Soft materials often exhibit nonlinearity, making the finite element method (FEM) a common approach for their analysis and solving continuum mechanical problems. Although FEM facilitates the analysis of complex structures with complex material

behavior, simulating such materials requires high computational costs.

The main objective of this study is to identify the key parameters of soft materials and their influence on the development of a material model based on inverse finite element method (iFEM) approach. By identifying these key parameters, an attempt is made to approximate the behavior of complex materials through a simplified material model and assess its potential future applications in medical research and its use with organs.

To achieve this goal, an experimental configuration will be selected, and a computational model will be developed to use an iFEM approach to identify the key material parameters of the given soft material. With this method, it was possible to match the results of the computational model to the experimental data, and validate the model with additional data points.

The objective of this study is to develop a framework that identifies the essential material parameters of soft materials and evaluates their limitations and impact on a validated model, which can describe nonlinear material behavior. By contributing to this framework, the study aims to accelerate the development of material models for practical applications in medical research and development.

## 1.3 State of the Art

This section reviews the state of the art relevant to this study. First, the experimental characterization techniques are reviewed, including methods for obtaining mechanical and viscoelastic properties. This is followed by the description of different approaches to describe the material model for different soft materials. Then, the iFEM, which is one method to identify material parameters from experimental data, will be explained. Finally, the standard verification and validation process used in computational solid mechanics for medical devices based on the American Society of Mechanical Engineering (ASME) guidelines will be discussed. The goal of this chapter is to provide a comprehensive overview of the current methods used in the field and the identification of limitations and gaps in the current state of knowledge.

### 1.3.1 Experimental Characterization for Soft Materials

Experimental testing is a key approach to obtaining information about the mechanical behavior of soft materials. In order to characterize the mechanical behavior of a test specimen, the most common method is to mechanically load the specimen and measure the response of the force against the displacement [2].

-Soft synthetic materials like soft gels are often used for tissue engineering applications. However, due to their

- Soft synthetic materials like soft gels are one example for soft synthetic materials. These are commonly applied for tissue engineering applications. Nevertheless, due to their elastic modulus range (kPa) present some challenges for the design of experimental testing [10].

#### Uniaxial Tension/Compression Testing

Uniaxial tension or compression testing are one of the most common methods to determine a stress-strain relationship. For uniaxial tension cases, usually the

specimen is well loaded in a machine by gripping the ends and performing tension tests. Then, the deformation is usually measured with a strain gauge [2]. As for compression test, the specimen is loaded by placing it in between from two plates and compressing the material [2].

In a study made by Kayanta and Ivankovic (2010), the authors investigated the behavior of an ether-based polyurethane elastomer for the production of mock arteries [7]. Polyurethane possesses excellent mechanical properties, like high elasticity and resilience and can be shaped in various shapes and sizes, making it a versatile material for the development of large arteries. For this material the uniaxial tests were performed using dumbbell-shaped specimens, and were divided into three groups based on the strain rates used (low, intermediate, and high).

Low strain rate tests were performed under a dry room temperature, wet room temperature, wet at 37 °C using a standard Instron machine

The uniaxial tension test was conducted using a custom-built apparatus that allowed for precise control of the applied load and measurement of the resulting deformation. The results of the test showed that the hydrogel material exhibited a nonlinear stress-strain behavior, with a rapid increase in stress at low strains followed by a more gradual increase at higher strains. These findings provide valuable insights into the mechanical behavior of hydrogels under uniaxial tension, which is important for understanding their behavior in various biomedical applications.

### Aspiration Experiment

Tissue aspiration experiments introduce an aspiration tube which is put against the soft tissue, generating a vacuum. An advantageous feature of this experiment is that it can be performed in-vivo and ex-vivo. With the help of a mirror placed next to aspiration hole, the reflection of the side-view of the tissue can be captured with a video camera. This camera captures the images of the illuminated surface of the material and the aspiration pressure is captured through a sensor. Through this process the captured profile of the tissue is obtained and this can be used to characterize the deformation and analyze the viscoelastic properties of the soft tissue[8].

### Indentation

Indentation has been gaining popularity in the last decades and it is now one of the most spread experiments for material parameter identification. Indentation presents a bigger advantage in cases where it is not possible to load test specimens in a more conventional way.[2] As some materials, e.g. biomaterials do not always allow the use of uniaxial or biaxial tensile testing, the use of indentation testing is essential.

Indentation possesses advantageous characteristics for the mechanical characterization of soft materials. [10] Nanoindentation or microindentation is useful for the evaluation of nonlinear viscoplastic responses. [2]

The indentation testing set up is described as follows: As shown in Fig. 1.1 A system applies a certain force to an attached indenter rod with a specific indenter tip. After the indenter tip goes to a determined displacement, it is possible to obtain a Load-displacement curve. The deformation can be measured through an capacitance gauge [2] or also optically (via laser measurements).

-indentation in materials - Indentation in soft materials (organs) - Why is indentation relevant in organs -what advantages and disadvantages does indentation provides - why is relevant for this project

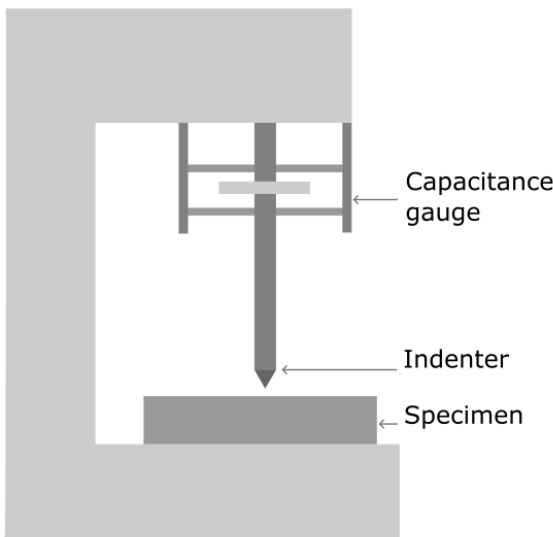


FIGURE 1.1: Nanoindentation experiment setup.

### 1.3.2 Material Modeling of Soft Materials

Relevant papers tends to use hyperelastic models to represent soft materials as the viscoelasticity is usually neglected. Material model are very relevant for the simulation model (Kauer2002). Soft tissues are approximated as near incompressible due to their highly water content. For the aspiration experiment conducted by Kauer they used the following strain energy function based on the model of Susanne and Bathe (SusanneandBAthe1987)

As derivative from this formula for the uteri metrial modeling the formula used was:

### 1.3.3 Inverse Finite Element Method for Parameter Identification

An inverse finite element (FE) approach requires usually a certain experimental model, which generates certain information e. g. load-displacement curve, and through a verified computational model match the given data curve to obtain further information of the material's behavior e. g., stress-strain curve.

Specially for nonlinear cases [5], where the complexity of the problems increases, and the interest is focused to generate an action which results in a certain output response, is where an inverse finite element approach can be helpful to discover a certain variable going from an ouput data. Through an iterative process it is possible to describe the material's behavior and validate the output data it through other established testing e. g., uniaxial testing.

Though this approach does not always give a hundred percent match in all obtain points or zones, it allows the researcher to understand the influences of certain parameters for the materials. This is specially useful for complex materials as biomaterials.

Biomaterials, as mentioned previously, depends on multiple external factors, e.g., blood pressure, affected diseases and the their material properties is constantly changing. This issue does not allow the researcher to develop a proper material model which is usable for multiple use-cases.

Therefore, the importance of the inverse element method as relevant key for estimating constantly changing parameters in soft materials.

For biomechanical models, where the models require knowledge from local properties [3], as the biomaterial is not isotropic; it is possible to identify a parameter e.g. Young's Modulus from a 3D model. The model can be matched to multiple experiments and multiple samples in different areas, which allows a better representation of the material for further analysis.

The inverse FE approach can be used by optimizing the searched parameter by matching the simulated data to a section of a experimental curve and extending this process through some iterations. Nevertheless, it is important to clarify that this method also requires making assumptions to some values. Furthermore, it is relevant to document these assumptions for the further analysis. With the combination of assumptions, experimental data, and a optimized and matched simulation curve, it is possible to solve the complexity of biomechanical models.

In next sections some of the experimental models and the material models for bio and soft materials are going to be explained to get a further understanding in how is possible to get a reliable computational model for further research

### Synthetic Soft Materials

Synthetics materials are commonly used to validate an inverse parameter identification process. Usually these synthetic, soft materials provide similar mechanical behavior to its biomaterials counterparts. This characterization allows to validate a proposed inverse finite element approach process before its applicatoin with a biomaterial, where the measurements to gather the experimental data are some in-vivo, and more challenging to recreate.

For example, Silgel, a very soft gel-like material [8] was used for the experimental validation of the inverse finite element method proposed, to characterized the tissue of a human uteri. In this work, the tensile behavior of the material was predicted through the parameters obtained in the aspiration method. The matching procedure is optimize through an objective function, which consists of the squared differences between the simulation and exprimental data. With an optimization algorithm an optimal set of the following parameters was found: the material parameters  $\mu_i$  [ $N/m^2$ ] and the bulk Modulus  $\kappa$  [ $N/m^2$ ]. This method showed good prediction quality of the mentioned material parameters.

### Biomaterials

Biomaterials as mentioned before, represent a challenge due its difficult access and lesser replicability. Therefore these materials are usually used for the experimetal validation of a methd applied previously in synthetic materials. Following the first example of the Silgel in the previous section, the inverse finite element parameter estimation is applied now on human uteri [8] through in vivo and ex vivo measurements of the human tissue of different patients. It was mentioned, that in comparison from the silgel the uterus possesses a complex multi layered structure with strongly anistropic and viscoelastic properties. Nevertheless, five material parameters were determined, based on the strain energy function to model a human uterus (Yamada 1970). Through the same inverse method applied with the synthetic material, the obtained parameters facilitated the prediction of stress-elongation curves for tensile experiments. The resulting curves showed the difference of stiffness for in vivo and ex vivo measurements and the material singularity for each uterus.

**1.3.4 Standard Verification and Validation for Computational Solid Mechanics (ASME)**

VV40

**1.4 Overview**

## 2 Experimental Model

The first phase of this project was to design and select an appropriate experimental model. This was essential to gather the necessary data from the tested material. This data will be used to determine the design parameters that can help to characterize the material's mechanical behavior.

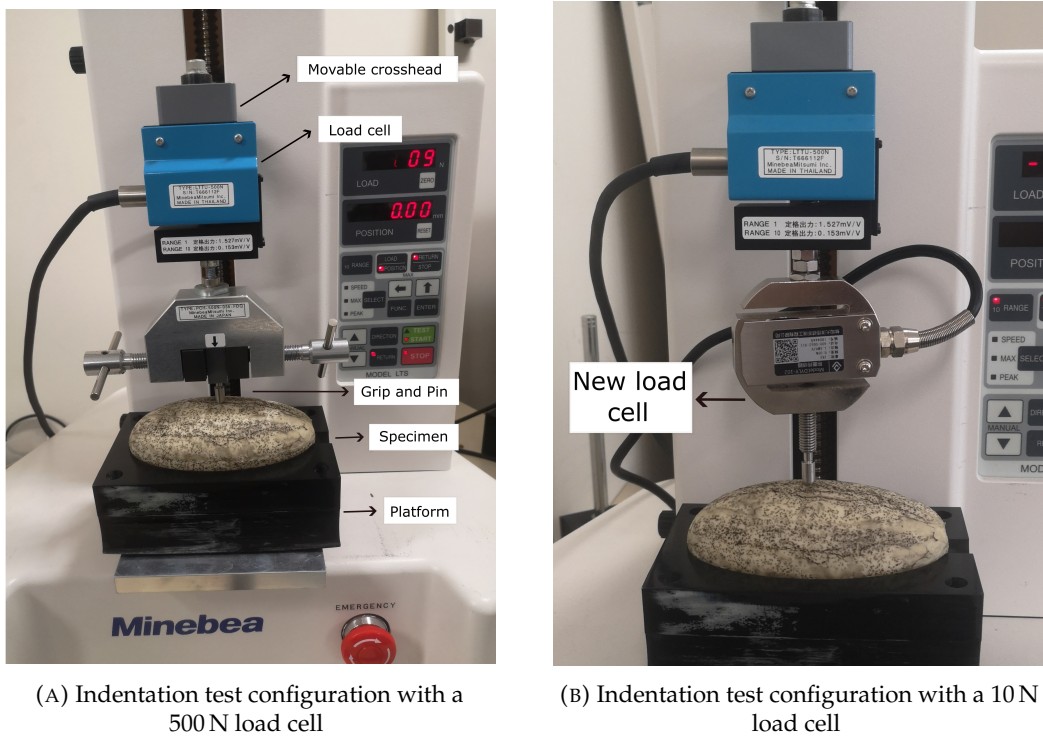
The experimental model I had the purpose of serving as a comparator for the experimental model II (see Section 2.2). At the beginning of the project, the desired experimental model to be analyzed was the second experimental model, which was developed and designed by Yokohama National University (YNU). As this second experimental model was still undergoing some improvements and corrections, a similar experiment was designed which could fulfill the same purpose.

The chosen experimental characterization for the inverse finite element method for the identification of material parameters for this project was indentation. The goal of these experiments was to observe the mechanical behavior of a soft material under compression using a rounded indenter. The aim was to determine the material behavior and observe the response under an indentation larger than the indenter radius. Additionally, by performing the indentation tests, the obtained data helped for a more in-depth understanding of the material's mechanical behavior for the chosen use cases and the determination of the main assumptions for the material modeling. The main advantage of indentation is the noninvasive feature, which will mostly become useful when a test sample should not be modified, e.g., an organ.

For both experimental setups, the specimen, which was tested, was made from a human skin gel. The human skin gel material was a two-component ultra-soft urethane resin. Polyurethane is widely used for biomedical applications, e.g., preparation of implants, wound dressings, artificial organs, and medical supplies.

Polyurethane can also be used for simulating organ tissues, as it can be tailored to mimic and match the mechanical properties of the desired biological tissues [14]. Furthermore, polyurethane can be synthesized to have a wide range of stiffness, elasticity, viscoelasticity, and can also be prepared with complex shapes for medical research purposes [6].

In this chapter, the different experimental models, which were used to evaluate the mechanical behavior of the ultra-soft polyurethane, will be described. In the first two subsections, will focus on the description and procedure of the experimental models, followed by explanation of the indentation test types. Consequently, an evaluation and analysis of the results will be provided and the main assumptions for the design of the material modeling will be defined.



(A) Indentation test configuration with a 500 N load cell

(B) Indentation test configuration with a 10 N load cell

FIGURE 2.1: First experimental model: Tensile and compression machine with an indenter with a rounded head. Test Specimen made from ultra-soft polyurethane resin positioned on a fixed platform with a similar shape for constraint.

## 2.1 Experimental Model I

### Description of the Experimental Setup

The first indentation test configuration was done by adapting a tensile and compression testing machine, model LTS - 500 NB from MinebeaMitsumi.Inc (Fig. 2.1). This machine possess a maximum load capacity of 500 N, and test speeds of 10 mm/min, 20 mm/min, 30 mm/min, 50 mm/min, 75 mm/min and 100 mm/min. To achieve an indentation testing configuration, a pin was attached to the movable crosshead holding grip, as shown in Fig 2.1a. The indenter had a rounded head made of stainless steel with a radius of  $r_{i1} = 3$  mm and a length of  $l_{i1} = 11$  mm.

The specimen possesses a ellipsoidal form with with a minor radius  $r_1 = 35$  mm and a major radius  $r_2 = 60$  mm. This specimen geometry is supposed to simulate a kidney with an extracted tumor; therefore, on the lower part of the specimen a half ellipsoid with a minor radius  $r_{l1} = 10$  mm and a major radius  $r_{l2} = 15$  mm was removed (Fig. 2.2). The specimen was prepared by a YNU laboratory member, by 3D printing a mold with the wanted dimensions and a ellipsoidal shape, and filling it with liquid resin. Additionally, it was left to cure for around 30 hours. It is relevant to clarify, that this sample had been created months before the development of this experimental setup and had been utilized in other projects conducted from the laboratory. This available specimen was positioned on a platform fixed to the base, which suited the ellipsoidal geometry for properly constraint.

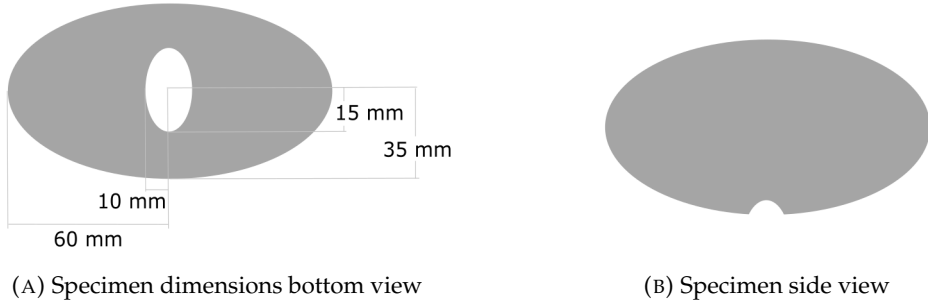


FIGURE 2.2: First experimental model: Specimen dimensions made from ultra-soft polyurethane resin for indentation test.

### Procedure for Conducting the Experiment

For the indentation test after placing the specimen on the platform, the indenter was positioned slightly on the surface of the point of interest. The test was conducted with a room temperature of approximately 22 °C. To perform the test the indenter was then lowered onto the surface of the specimen at a velocity of 10 mm/min. The indentation depth was controlled by limiting the maximum depth, and the test stopped once the inserted depth was reached. The indenter returned to its original position after reaching the maximum depth with a rate of 100 mm/min. Due to the material properties, the specimen returned to its original shape. The result of the indentation test was a load-displacement data, which was recorded with a sampling rate of 63 Hz using a load cell of  $\pm 500$  N and a encoder to measure the displacement.

The measurement accuracy according to the specification of the machine, has a relative reading error of 1.0 %. The indentation test was repeated five times on the same sample to ensure and observe reliability and repeatability. Furthermore, the raw data collected from the test was processed and analyzed using Excel.

During the initial indentation test using the 500 N load cell, the collected experimental data showed noise that could affect the accuracy and reliability of the results. The noise was likely caused by sensitivity of the lead cell. The ultra-soft polyurethane material showed force readings, which were near the lower limit of the load cell's range, which adding any other external factors, results in noisy measurements. To address this issue, a load cell of 10 N was installed (Fig. 2.1b). This change improved the quality of the measurements and reduced the noise in the data. The change to the load cell had some implication to the experimental setup, such as removing the holding grip, and designing a part which could connect the indenter with the new load cell. In addition to changing the load cell, a simple filtering method was used to improve the experimental data. After applying the filter, the noise in the data was reduced, resulting in more smoother force reaction readings.

The applications of the combinations helped to improved the quality and accuracy of the data and gave important information about possible measurement errors to take into consideration for of the experimental model designed by YNU. At last, The filtered data was used for subsequent analysis and interpretation for the inverse finite element method approach for the material parameter identification.

## 2.2 Experimental Model II

The second experimental model was developed and designed by Yuta Mori, a member of the Yamada Laboratory from the Mechanical Engineering department of Yokohama National University. The main aim for this experimental method was to be able to identify the physical properties of organs in a state that closely resembles the *in vivo* environment. Additionally, this model sought to achieve two objectives: firstly, to develop a loading system to acquire the data required for an inverse analysis, and secondly, to establish a measurement process in case of a total nephrectomy [11].

Furthermore, for the present experimental setup a new sample was prepared using the same material as the previous one, i.e., human skin gel made from ultra-soft polyurethane resin, and following the same manufacturing process as described in Section 2.1.

The resulting data from the experimental model served for the basis of the material parameter identification for the inverse finite element method approach. The processed data obtained from this experimental model assisted in the calibration and assessment of the design parameters employed in the validation for the computational model.

### Description and Procedure of the Experimental Setup

In this experimental model the indentation loading system, which gathers data of the indentation depth, reaction force and general deformation. The experimental device consists of a 6-axis force sensor, a laser displacement transducer, and 3D cameras placed in four directions to obtain the point cloud data based on the coordinate system of each camera. Fig.2.3 shows the setup of the experiment. For our project, the 6-axis force sensor and the laser displacement were mainly used. The loading system is operated by specifying the movement of the loading rod in advance, and the indentation is performed in the direction normal to the contact surface to prevent slippage (Fig. 2.4).

The specimen, same as in the first experimental model (Section 2.1), possessed the same dimensions, a minor radius  $r_1 = 35$  mm and a major radius  $r_2 = 60$  mm, and was made from ultra-soft polyurethane resin. Consequently, the platform is also bowl-shaped. For this experiment, the platform base was made from transparent acrylic resin to record the contact status of the bottom surface [11]. The maximum load capacity of the load cell is 200 N and a theoretical force resolution of 0.001 N. In addition, the resolution of the laser displacement sensor is 0.05 mm. The indenter is sphere-shaped with a radius of  $r_{i2} = 3$  mm and was made from ruby with the following specifications; a Young's Modulus of  $E_{i2} = 440$  GPa and a Poisson's ratio of  $\nu_{i2} = 0.3$  mm.

The indentation test was conducted under room temperature conditions. Also, the sample was placed on acrylic platform and the indenter was lowered at constant velocity of 30 mm/min. The experiments were conducted for each loading point five times on the same sample, and the average of the results were calculated.

Furthermore, to minimize the friction during the indentation process, the indenter and the loading surface on the specimen were covered with a thin layer of lotion. This was done due to inaccuracies and step-like data shown in the measurements. Therefore, to reduce this measurement error, the application of lubricant was

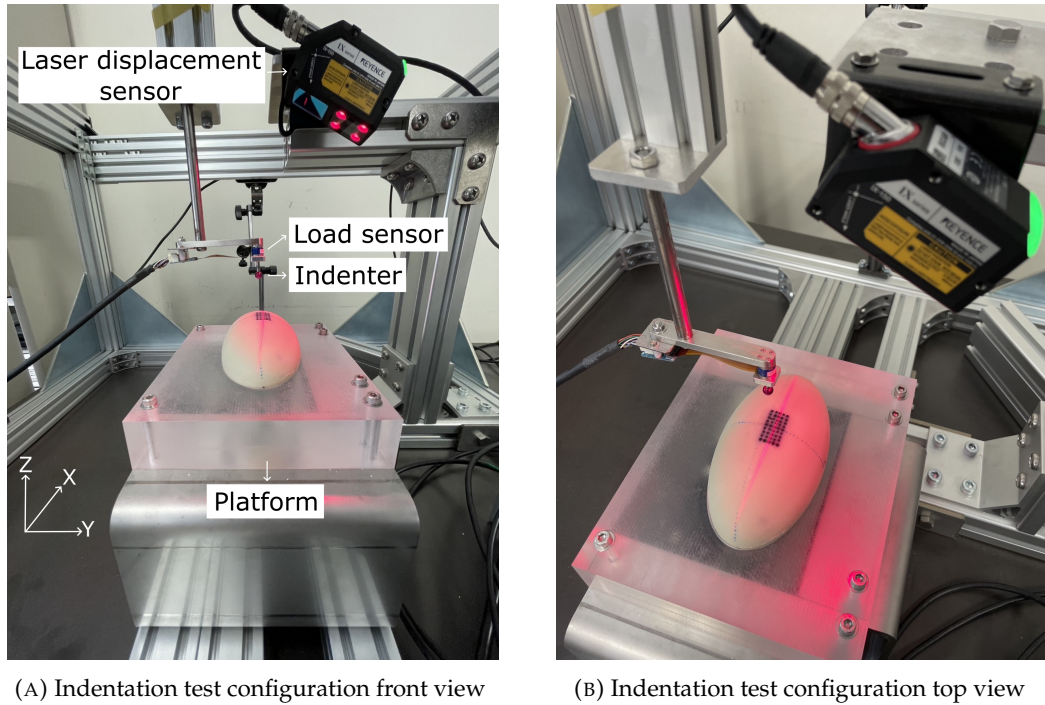


FIGURE 2.3: YNU experimental model: 6-axis sensor Test Specimen made from ultra-soft polyurethane resin positioned on a fixed platform with a similar shape for constraint.

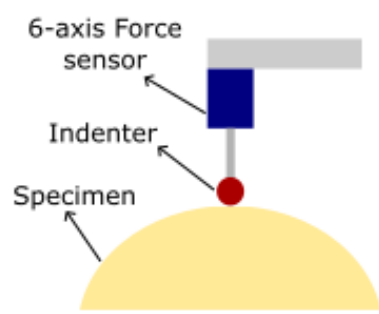


FIGURE 2.4: YNU experimental model: Loading diagram showing initial position of the indenter in normal position [11].

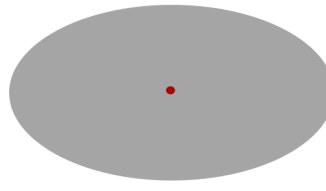


FIGURE 2.5: Middle test point: Loading point on the top surface of the specimen.

employed, ensuring a smoother and more controlled indentation process. Finally, the data was also processed and assessed using Excel.

### Analysis and Comparison of Experimental Techniques

The second experimental model offers some advantages over the first model. Firstly, it enables not only the measurement of the total force reaction, but also the analysis of the force reaction components  $F_x$ ,  $F_y$  and  $F_z$ . This allows for a better understanding of the material's mechanical behavior, as it allows the identification of a specific contribution of the force components and it contributes to identify other mechanisms such as viscoelasticity, plasticity, and creep. In addition, the second model allowed for the measurement of the deformation in other points near the tested loading point. This provides additional information of the material parameters, as it facilitates the characterization of the deformation behavior beyond the direct vicinity of the indentation point. Furthermore, only this test configuration makes use of a lubricant, as this experimental setup could show some inaccuracies in the first data sample.

In contrast, the first experimental model only measures the total force reaction against the indentation depth, without providing any information about the contribution of each component. While the first model allows the data gathering in simpler and more straightforward way, it may not capture the whole complexity of the material.

## 2.3 Experimental Tests Description

### 2.3.1 Middle Point

The first use case for the indentation test was performed at the midpoint of the major and minor axis of the ellipsoid (Fig. 2.5). This point was selected to ensure that the indentation was normal to the surface, thereby avoiding the influence of potential shear forces which could influence the measurements.

Additionally, the first indentation depth was chosen arbitrarily, for the first experimental model was  $h_I = 3.8$  mm, and for the second experimental model was  $h_{II} = 4$  mm. This depth was considered to be an appropriate compromise that would allow to capture the nonlinear behavior of the material, while also remaining a simple use case to reproduce in a computational model in ANSYS.

As the main objective is to find a path, which lets identify the material parameters, the most basic use case was selected and from this point the complexity was gradually built on. Through this approach, it was possible to establish a solid foundation for the subsequent experiments and data analysis.



FIGURE 2.6: Load-Unload Case: Experimental model I with modified configuration setup, on top of the movable crosshead a displacement transducer was equipped to capture unloading data.

### 2.3.2 Load-Unloading

Building on the previous test point (Fig. 2.5), an indentation test was conducted on the same point, with an indentation depth of 4 mm, but this time in a loading-unloading case.

The first experimental model setup, as described in Section 2.1, was unable to measure the displacement and force reaction during the unloading of the specimen. As a result, certain modifications were made to the experimental setup. Due to time constraints, the modification of experimental model I was also executed by laboratory members Mori Yuta in YNU. To capture the displacement and force reaction during the unloading, a displacement transducer was equipped to the tensile and compression machine as shown in Figure 2.6.

The aim of this use case, was the observation of a possible hysteresis behavior, as well as to investigate the viscoelastic properties of the material. The load-unload test was performed at six different loading speeds, namely, 10 mm/min, 20 mm/min, 30 mm/min, 50 mm/min, 75 mm/min and 100 mm/min on the same specimen. Each speed configuration was repeated five times, and the results were averaged to reduce the effects of experimental variability.

The load-unload case helped to determine whether complex material behavior such as viscoelasticity, could be neglected for the computational model of the middle point test. The results of this experiment were used to make this decision, which has important implications for the simplification of the computational model and its accuracy and reliability.

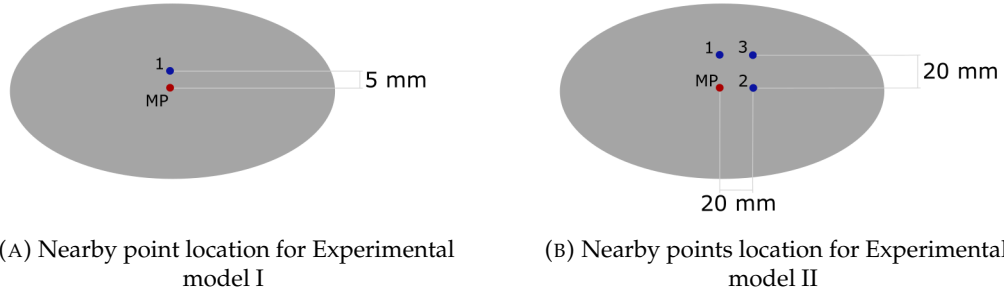


FIGURE 2.7: Nearby test point: Loading points for each experimental model to analyze shear stresses and to validate employed for the validation of the computation models.

### 2.3.3 Nearby Point

In addition to the indentation performed on the middle point of the surface, further indentations were conducted on nearby points. From these indentation tests, force-displacement curves were recorded. For each indentation the same experiment configuration, e.g., indentation depth and indentation speed, was employed as described in Sections 2.1 and 2.2.

For the first experimental model, only one nearby point located  $p_{I1} = 5 \text{ mm}$  to the right of the middle point was selected as shown in Figure 2.7a.

For the second experimental model, three additional nearby points were tested. These points were located at distance of  $p_{II1} = 20 \text{ mm}$  to the right,  $p_{II2} = 20 \text{ mm}$  downwards, and a third point  $p_{II3} = 28.3 \text{ mm}$  diagonally from the middle point forming a square (Fig. 2.7b).

The objective of these testing points was to gain a deeper understanding of the effect of the shear stresses on the indentation response. Furthermore, the results of these points allowed for the validation of the computational model and the selected material model.

## 2.4 Analysis and Overview of the Data and Results

In this section, the results of the experimental models described in the previous sections will be presented and analyzed. The objective is to understand the behavior of this ultra-soft polyurethane material under indentation and establish the first assumptions for the development of the computational model, as well as the material model. The section will start with a brief summary of the tests, followed by the analysis of the force-stroke curves gathered throughout the experiments.

The experimental model I served mainly as a comparator and a quick way to gain an idea of the mechanical behavior under indentation, for this model three different use cases were measured. An indentation in the middle point of the surface with an indentation depth of  $h_I = 3.8 \text{ mm}$ . Subsequently, the load-unload case was observed under an indentation depth of  $h_{I2} = 4 \text{ mm}$ , and with six different speeds ranging from  $10 \text{ mm/min}$  to  $100 \text{ mm/min}$ . Finally, a nearby point was selected near the middle point,  $p_{I1} = 5 \text{ mm}$  to the right, to use it as a validation point for the selected material model.

A similar process was followed for the experimental model II, the middle point indentation was performed with an indentation depth of  $h_{II} = 4 \text{ mm}$  and a indentation speed of  $30 \text{ mm/min}$ , where the force components could be observed. Similarly, the load-unload scenario was tested under the same conditions, and three nearby points were measured.

### 2.4.1 Middle Point

The results of the indentation test at the middle point for both experimental showed a clear nonlinear behavior. It is assumed that this material possess a elastic-plastic behavior, which in a typical load-displacement curves has four known stages [4]:

1. Nonlinear elastic (self-adjusting): In this stage, the material adjusts itself to the loading conditions, and the deformation is elastic and reversible.
2. Linear elastic: The material is bearing the external load in this stage, the deformation is still elastic and reversible
3. Nonlinear plastic (failing): With the increase of the external load, the material reaches its yield point and undergoes permanent deformation
4. Failure: The material fails leading to permanent damage.

Figure 2.8 shows the results of the two indentations at the middle point of the specimen surface. The load-displacement curves showed nearly identical material behavior for both experimental configurations. This use case demonstrate the nonlinear-elastic behavior of the material, as there was no evidence of a yield point or plastic behavior. Both curves began at zero, and the force increased gradually with increasing, resulting in a slightly concave shape.

Figure 2.8a displays all the measurements points obtained from experimental model I and its polynomial approximation. This approximation was used for the subsequent steps of the iFEM approach. The maximum total force for experimental model I at a maximum indentation depth of  $u_{I,MP} = 3.8 \text{ mm}$  was  $F_{I,MP} = 0.4218 \text{ N}$ . For experimental model II, at an indentation depth of  $u_{II,MP} = 4 \text{ mm}$ , the maximum forces for each component were  $F_{Z,II,MP} = 0.546 \text{ N}$ ,  $F_{Y,II,MP} = 0.0124 \text{ N}$ , and  $F_{X,II,MP} = 0.0093 \text{ N}$ .

From load-displacement curve of experimental model II (Fig. 2.8b) it was evident that the force reactions in the X and Y directions could be disregard, as these were considerably lower than the force reaction in Z direction. Therefore, the focus in further analysis was mainly on the force reaction in Z direction. Additionally, this case revealed that shear stresses were minimal, which is consistent with the purpose on performing the indentation with the least influence of external factors.

Figure 2.9, shows that the load-displacement curve of experimental model I has a similar initial behavior to that of experimental model II. However, as the indentation depth increases, the curve of experimental model I is positioned lower than that of the second model. One possible explanation for this difference could be the effect of aging on the material properties of the specimen used in the first model. Since the specimen used in this configuration was manufactured months before (Section 2.1), it is possible that the aging had led to a decrease in its mechanical properties, resulting in a lower resistance to deformation and therefore, lower stiffness than the newly manufactured sample. Another possible explanation could be the presence

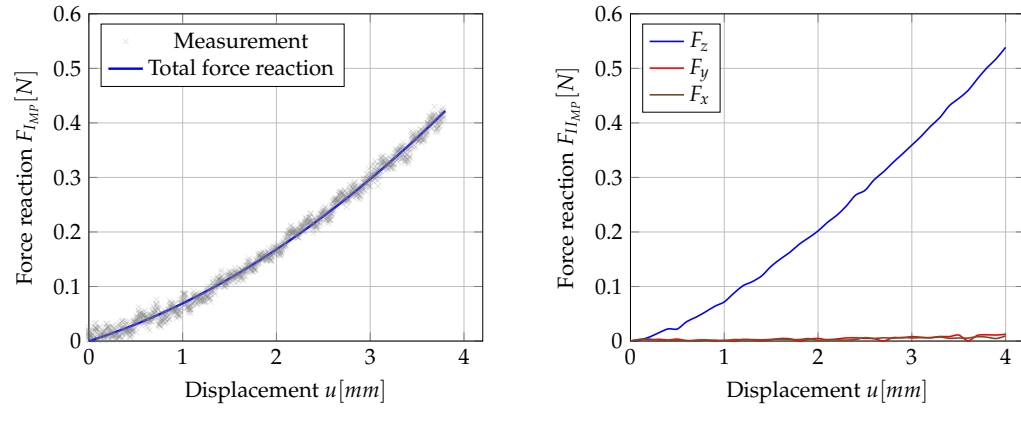


FIGURE 2.8: Load-displacement curve experimental data for Middle Point use case for both experimental models.

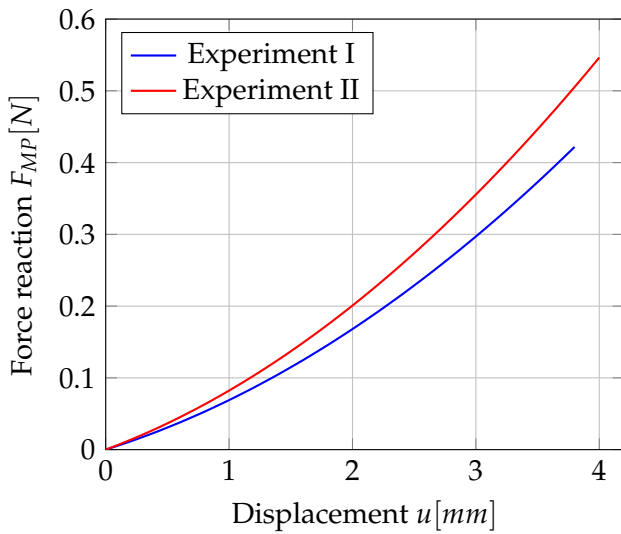


FIGURE 2.9: Total Force Reaction-Displacement curve: Comparison between experimental data for Middle Point use case from both models.

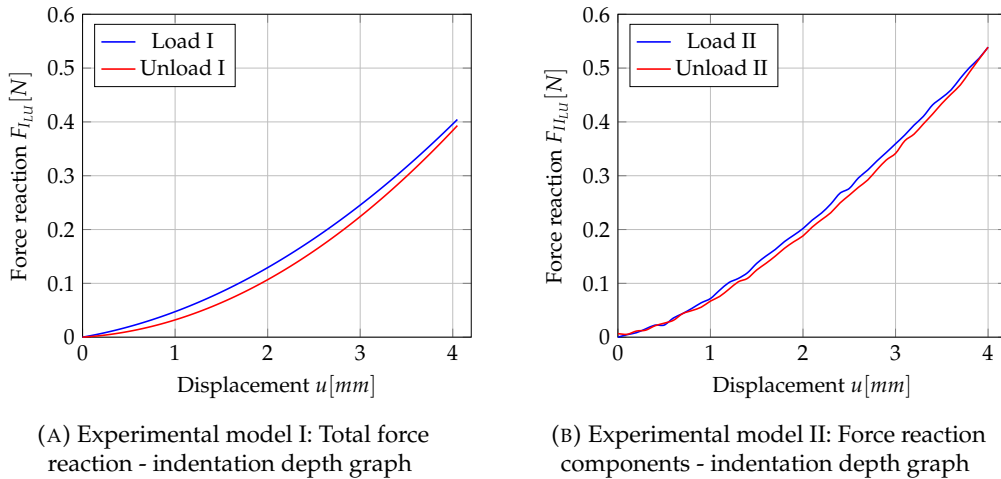


FIGURE 2.10: Load-displacement curve experimental data for Load-Unload use case for both experimental models.

of external factors during the conduction of the experiments or the configuration of these. Nevertheless, as the main purpose of this Middle Point use case was to minimize the influence of these factors, this explanation seems less probable.

#### 2.4.2 Load-Unloading

Following the Middle Point use case, in addition to the loading data, the unloading was also captured for both experiments as explained in Section 2.3.2. Figure 2.10 shows the load-displacement curve for experimental model I and next to it experimental model II. Both results exhibited during the unloading some degree of hysteresis, as there was a slight difference in the force reaction measured. However, the material displayed good elastic behavior, as it returned to its original shape once the indenter was removed.

The hysteresis displayed for both configurations could have occurred due to several reasons, such as viscoelastic behavior of the material, or external factors, like friction between the indenter and the specimen, surface roughness of the indenter, test configuration, and so on. To examine closer the main reason for the hysteresis, only with first experimental setup, a series of indentations tests were performed with different speeds.

Figure 2.11 shows the result of the load-unload indentation tests from the lowest to highest value for the indentation speed. It could be observed, that the curves exhibit a similar material behavior. A slight increase in the hysteresis was observed when the indentation speed was increased. Specifically, during the loading, the force reaction were slightly higher as the speed and indentation depth increased. During the unloading, the only notable difference was observed with 100 mm/min, where the unloading curve had the lowest values.

From the results and in the case of ultra-soft polyurethane, it is likely that the hysteresis is primarily due to the viscoelastic behavior of the material. Nevertheless, for the tests done in the middle of the surface, it was decided that the viscoelastic properties could be neglected for the material modeling seeing that the difference between the curves is not impactful for the first stage of the identification of the material parameters.

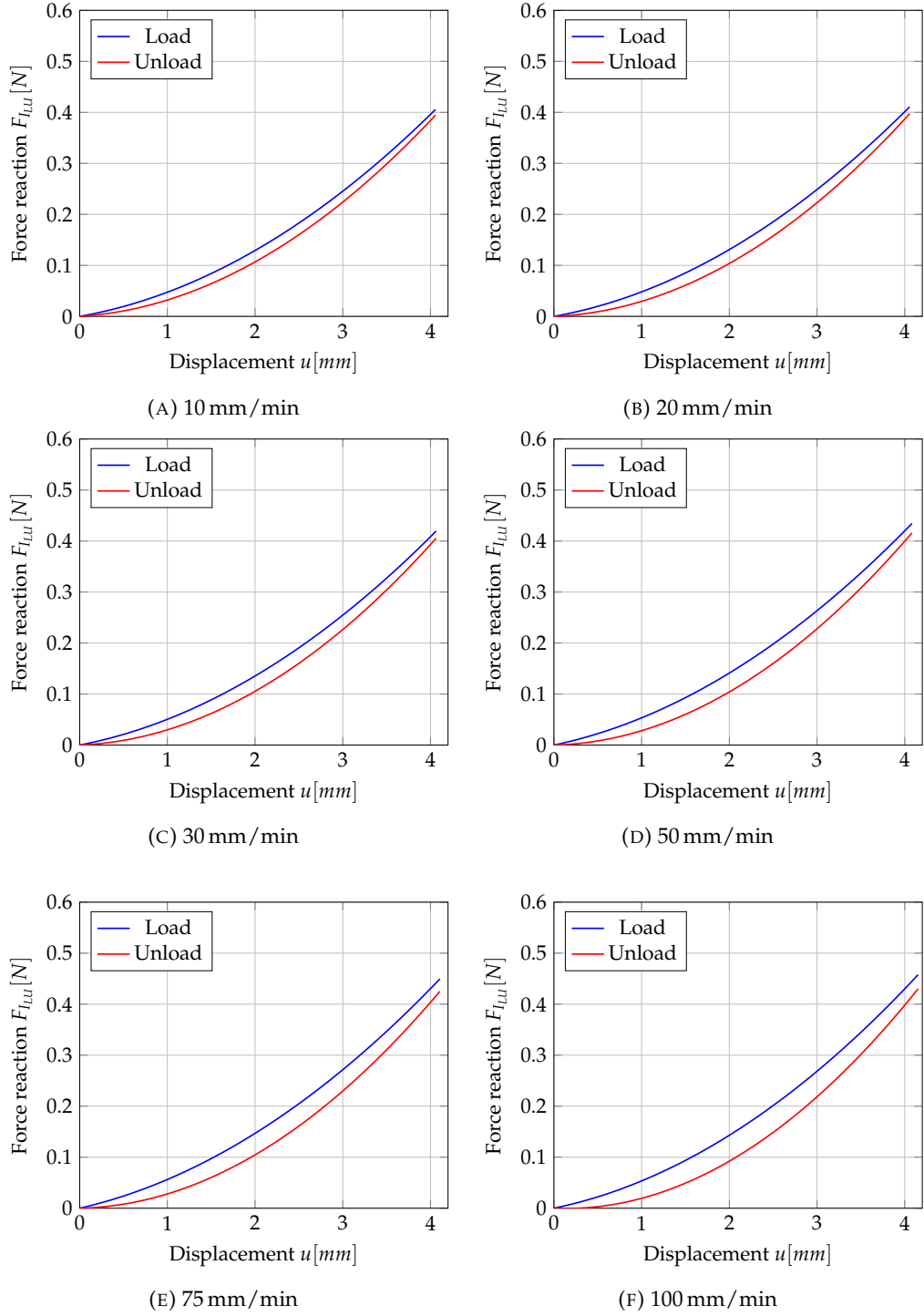


FIGURE 2.11: Load-Unload Use Case: Analysis of Viscoelastic material properties by using six different indentation speeds. Load-Displacement curves were obtained from the first experimental test configuration.

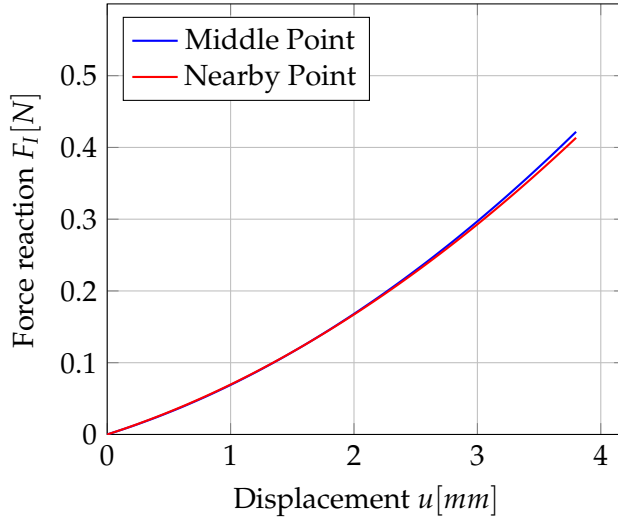


FIGURE 2.12: Total Force Reaction-Displacement curve: Comparison between experimental data for Middle Point and Nearby Point. This point was located 5 mm right from the midpoint, following the minor axis of the ellipsoid.

#### 2.4.3 Nearby Point

To complement the analysis of the viscoelastic behavior of the material, a nearby point located  $p_{I1} = 5$  mm to the side of the midpoint, following the minor axis of the ellipsoid (see Subsection 2.3.3). This location was chosen to investigate if the mechanical response of the material is uniform across the surface and if any variations could be detected within a short distance. Figure 2.12 shows the results of the Middle Point use case vs. the selected Nearby Point case for experimental model I.

The new load-displacement shows nearly identical behavior to that of the first case, except for the last part of the curve, where the Nearby Point curve goes slightly lower. The maximum force obtained for the Nearby Point case was  $F_{I_{NP}} = 0.4134$  N, which is lower than the one obtained before, which was  $F_{I_{MP}} = 0.4218$  N.

It can be concluded, that the results from this nearby point support the findings from the Middle point test, indicating that the material behavior was homogeneous in the region of interest. The small difference in the maximum force values could be due to the variations in the experimental conditions, e.g. the increment of the gradient of the contact surface due to the curvature of the specimen. This change could potentially affect the distribution of the stress and strains within the material. Nonetheless, these differences were not significant enough to affect the overall conclusions.

With the measurements taken in the additional nearby points for experimental model II (Subsection 2.3.3), it was possible to investigate whether the small variations in the results obtained with experimental model I could be attributed to the difference in the gradient of the contact surface. Figure 2.13 shows the result for each force reaction component for all four tested points. In X-direction, the maximum force was observed for point 2, which had the smallest gradient contact surface, followed by point 3. These points were 20 mm down along the X-axis, in contrast to the other two points, which were at the origin of the X-axis. For the middle point

and point 1, which had the largest contact surface gradient, the X-component force reaction was almost 0 N.

Similarly, in Y-direction, the maximum force was observed for point 3, followed closely by point 1. For the middle point and point 2 the Y-component force reaction was almost 0 N. Point 3 and point 1 were 20 mm right along the Y-axis, and the middle point and point 2 were at the origin of the Y-axis. As for the Z-direction, the maximum force was observed at the middle point, followed by point 2, and consequently with similar results point 1 and point 3. For all the points the results in Z-direction are more significant than in the other directions.

These results suggested that variation in the gradient of the contact surface may have contributed to the small differences in the results obtained with experimental model I. Specifically, it was observed, that with a smaller contact surface gradient the higher the X-component the same for the Y-component with the larger contact surface gradient. In conclusion it is possible to confirm that the material behavior was homogeneous, and that the larger the contact surface gradient became, the lower the total force reaction.

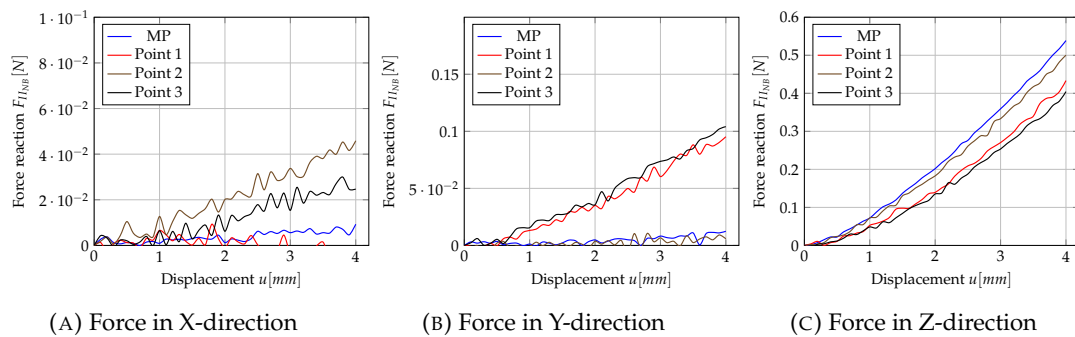


FIGURE 2.13: Nearby Point Use Case: Analysis of shear stresses by observing three different nearby points on the specimens surface. Load-Displacement curves were gathered from Experimental Model II showing each force component.

## 2.5 Main Assumptions for Material Modeling

In this section, the main assumptions based on the results obtained from the indentation tests will be summarized. These assumptions will be used for the development of the material models. As previously mentioned, one of the goals of this project was to develop the material model from an ideal scenario, while considering the limitations at each level. The complexity of the material model was incrementally increased until a set of material parameters that provided a proper compromise to the experimental results was obtained. Defining these levels allowed the assessment of the impact of each parameter on the development of the material model.

Based on the presented experimental data and previous discussion, the following assumptions could be made:

1. The material can be assumed to be homogeneous in the region of interest for the Middle Point Case, as the results from the nearby points support the findings from midpoint test.

2. Nonlinear elasticity is observed and hysteresis can be neglected, as the changes observed with the different loading speeds were not significant enough to affect the initial results.
3. The viscoelasticity of the material can be ignored for the first design of the material model, as the material returns to its original shape and almost no energy is lost during deformation.
4. Friction and shear stresses will be neglected, as in the Middle Point case the observed force components in x and y directions are non-relevant.

It is important to mention, that it was noted that the main assumptions made may not hold for different experiment settings, such as higher loads, longer loading times, higher temperatures, high shear stresses, and so on. Therefore, it was important to keep these assumptions in mind when using the chosen material model in a validation case.

### 2.5.1 Level 1: Linear elasticity

The first level a linear elastic model was used. This model assumed that the material behaves linearly, i.e., the deformation is linearly proportional to the applied load and the material returns to its original shape after the load is removed. This model is based on Hooke's law, where the stress-strain relationship is

$$\sigma = E\varepsilon,$$

where  $\sigma$  is the stress,  $E$  is the elastic modulus, and  $\varepsilon$  is the strain. For the Middle Point Case, the material is assumed homogeneous and isotropic, thus the elastic modulus is the same in all directions. For an indenter with a spherical tip, the contact area  $A$  between the indenter and the specimen can be approximated as,

$$A = r_i^{\frac{1}{2}} h^{\frac{1}{2}},$$

where  $r_i$  is the radius of the indenter, and  $h$  is the indentation depth. For a spherical indentation assuming the Hertzian contact theory, the Hertzian relationship between the applied force  $F$  and the indentation depth  $h$  is [9],

$$F = \frac{4Er_i^{\frac{1}{2}}h^{\frac{3}{2}}}{3(1-\nu^2)}, \quad (2.1)$$

where  $E$  and  $\nu$  are the Young's modulus and Poisson's ratio of the indented material. This Hertzian relationship is used as the analytical basis on the contact of ellipsoid bodies in indentation experiments [9]. This model provided a simple and straightforward approach to describe the material behavior under small deformations. The elastic modulus and the Poisson's ratio are the two main parameters that will be used for this model. Additionally it was assumed that the material is near incompressible, therefore, a fixed Poisson's ratio was chosen,

$$\nu = 0.49, \quad (2.2)$$

leaving the analysis of one parameter, the elastic modulus. The linear elastic model served as a basis for the more complex material models developed in the subsequent levels, and it provided a reference point for the identification of other material parameters.

### 2.5.2 Level 2: Hyperelasticity

The second level introduces a higher complexity, as more material parameters are analyzed. For this level a Neo-Hookean model was used to describe the material behavior based in the strain energy potential function. The elastic strain energy potential function for the Neo-Hookean material model is given by

$$W = C_1(I_1 - 3) + \frac{1}{D_1}(J - 1)^2, \quad (2.3)$$

where  $C_1$  is a material constant,  $D_1$  the material incompressibility parameter,  $J$  the determinant of the elastic deformation gradient, and  $I_1$  is the first invariant of the right Cauchy-Green deformation tensor, i.e.

$$I_1 = \lambda_1^2 + \lambda_2^2 + \lambda_3^2,$$

where  $\lambda$  are the principal stretches [12]. To maintain conformity with linear elasticity, the material constant

$$C_1 = \frac{\mu}{2}, \quad (2.4)$$

where  $\mu$  is the shear modulus or the second Lamé parameter. If the material is assumed to be incompressible,

$$J = 1,$$

and the second term in the strain energy potential  $W$  becomes zero [13].

The Neo-Hookean model requires two main parameters to be identified; the shear modulus  $\mu$  and the incompressibility parameter  $D_1$ . The incompressibility parameter relationship with the initial bulk modulus

$$K = \frac{2}{D_1}, \quad (2.5)$$

can be defined [1]. The relationship between the shear modulus, the elastic modulus, and the Poisson's ratio

$$\mu = \frac{E}{2(1 + \nu)}, \quad (2.6)$$

can be calculated, as well as for the bulk modulus

$$K = \frac{E}{3(1 - 2\nu)}. \quad (2.7)$$

Using the results of the first level with  $E$  and  $\nu$  it is possible to establish a possible range for  $\mu$  and  $D_1$ . This targeted range helped in the reduction of computational time for simulations. The hyperelastic model provides a more accurate description of the material behavior in comparison to linear elastic model, as this model takes into account the nonlinear behavior of the material.

# 3 Computational model

## 3.1 Middle point

### 3.1.1 Description

The quasi static nature of the indentation experiment allows the use of a static structural analysis.

For the creation of the computational model, the SOLID 187 elements were used. The mesh for the whole model is formed from quad tetrahedral elements. The platform and the specimen have a global element size of 5 mm. The indenter has an element size of 0.5 mm. In the area of the indentation, there is finer mesh with an element size of 1 mm and a radius of 8 mm.

### 3.1.2 Analysis and Complications

There are two main factors which increase the complexity of the validation of the simulation and those are, the contact nonlinearity, and the element distortion due to indentation experiment. These issues make the computational time expensive, as it requires manual solutions for the meshing in the area of importance, and small time steps. For that, the nonlinear adaptive meshing option in ANSYS Workbench was applied, which does a remeshing process if a certain parameter is exceeded. Specially, for larger indentation cases, this option shows a more stable model with a good mesh convergence analysis.

A force-displacement curve, shown in Fig... is generated from the first assumption, for this case

For both cases

### 3.1.3 Verification of the Simulation Model

#### Mesh Convergence Analysis

#### Platform vs Fixed Support

## 3.2 Nearby point



# 4 Inverse Finite Element Method for Material Parameter Identification

## 4.1 Procedure of IFEM

## 4.2 Material Modeling

In an ideal and first scenario, this material can be assumed as linear, isotropic, elastic and nearly incompressible. For this case, there are two main variables, the Young's Modulus  $E$ , and the Poisson's ratio  $\nu$ .

From the parametric analysis, it is possible to see that the bulk modulus of this material does not possess a big impact in the FE simulation results. This conclusion combined with the results from the Poisson ratio in the first material model coincide with the statements from Bergström, where it is no vital to know these parameters to obtain accurate FE computational models, as these have limited influence on the mechanical response. [2]

### 4.2.1 Response Surface Optimization

#### Linear Elastic Model

#### Hyperelastic Model: Neo-Hookean

### 4.2.2 Objective Function Optimization

### 4.2.3 Analysis and Comparison of Each Approach



# 5 Results

## 5.1 Overview and Analysis

## 5.2 Framework proposal

## 5.3 Verification and Validation

### 5.3.1 Deeper indentation

### 5.3.2 Deformation profile analysis

## 5.4 Limitations and implications of the results

### 5.4.1 First Experimental model

The chosen experimental technique for the inverse identification for this project was indentation. The test specimen used for this experiment was a ultra-soft polyurethane resin. As shown in Fig.. the specimen possesses a ellipsoidal form with with a minor radius  $r_1 = 35$  mm and a major radius  $r_2 = 60$  mm. This was positioned on a fixed platform that suited the ellipsoidal geometry of the specimen to constrain its movement. The specimen was tested in a indentation test configuration with a tensile/compression machine. To achieve this congiguration a pin with a rounded head made of structural steel, with a radius of  $r_3 = 3$  mm was attached to the holding grips followed by a force load cell. The result of indentation test was a load-displacement points. The approximated polynomial curve was used as a reference for the material modeling.

The measured force reation  $F_1$  data showed a very small number, so the first 50 N load cell displayed a lot of noise in the measurements. Therefore, the load cell was change to 10N to reduce this interference. The 10 N load cell displayed the force-displacement curve of the indenter and the specimen in a finer way. Furthermore, in order to get the measurement of the load and unloading process of the indentation a displacement sensor was attached to the tensile machine.

The indentation depth  $h_1$  selected for the first model was 3,8 mm on the middle of the top surface of the specimen. This indentation depth surpasses the pin radius  $r_3$  and was chose arbitriarily to analyze the behavior of the material on the defined position. Additionally, it was observed that in soft materials it is easier to capture some parameters with a larger indentation. Some references also observe that with indentation depth lower than indenter radius has a lot of noise and do not describe th results accurately.

From the first experimental model we can observe that the material shows a non-linear behavior and the maximum total force reaction  $F_1$  lies around 0.45 N. Furthermore, when applying different speeds, as show in Fig. it is also possible to observe that the hysteresis increases. This increasement shows that the material possesses a viscoelastic behavior, however as this increasement is not significantly, it is possible to neglect viscoelasticity for the first stages of the project.

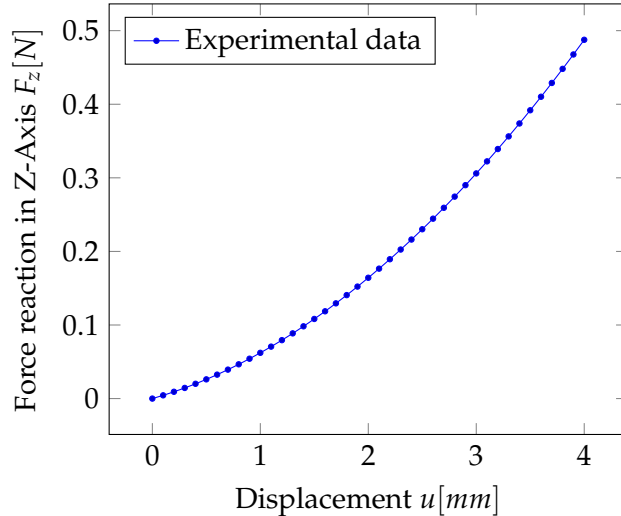


FIGURE 5.1: Experimental Load-displacement curve.

#### 5.4.2 Second Experimental model

The second experimental model was developed by Yokohama National University. Similar to the first experimental model the test specimen and the platform were it lies, has the same dimensions, minor radius  $r_1 = 35$  mm and a major radius  $r_2$  of 60 mm. The test specimen is also made from the same material, ultra-soft polyurethane resin.

The indenter on the other hand, is a sphere made of ruby, the sphere radius is also equal to the radius of the pin  $r_s$  3 mm and attached to it, is the force load cell.

A laser is used to measure the displacement which results in a load-displacement curve. With this model it is possible to not only determine the total force reaction, but also its components  $F_x$ ,  $F_y$  and  $F_z$ . Furthermore, with the laser it is also possible to observe the deformation not only in one point but around the whole area. This allows as to analyze the deformation of the whole structure.

The indentation speed selected was and with an indentation depth of  $h_s$  is 4 mm. With this experiment, 4 key points on the specimen's surface were chosen: First, in the middle and three other points, one to right, one down, and one diagonal to middle, forming a square with a distance between points of  $d_s$  20 mm.

Similar to the previous model, Fig. shows a nonlinear behavior with a maximum force reac

### 5.5 Material model framework assumptions

The first point to be analyzed, which is used to build a material model is point No. 1, in the middle of the surface. The advantages from this case, is the less influence of external factors. For this case it is viable to assume, that shear stresses can be neglected and offers a simple model to focus on the material definition.

For this project, there is a focus on the limitation of each material model, departing from an ideal scenario. From this point on the material will be built accordingly and for each model the influence of the material parameters is going to be assessed.

### 5.5.1 First Material model

**Linear elasticity**

**Hyperelasticity**

The strain energy density function for the Neo-Hookean material model is given with

$$\Psi = C_1(I_1 - 3),$$

where  $C_1$  is a material constant and  $I_1$  is the first invariant of the right Cauchy-Green tensor. Neo Hookean and Mooney Rivlin comparison

## 5.6 Computational model

The quasi static nature of the indentation experiment allows the use of a static structural analysis.

For the creation of the computational model, the SOLID 187 elements were used. The mesh for the whole model is formed from quad tetrahedral elements. The platform and the specimen have a global element size of 5 mm. The indenter has an element size of 0.5 mm. In the area of the indentation, there is finer mesh with an element size of 1 mm and a radius of 8 mm.

There are two main factors which increases the complexity of the validation of the simulation and those are, the contact nonlinearity, and the element distortion due to indentation experiment. These issues make the computational time expensive, as it requires manual solutions for the meshing in the area of importance, and small time steps. For that, the nonlinear adaptive meshing option in ANSYS Workbench was applied, which does a remeshing process if a certain parameter is exceeded. Specially, for larger indentation cases, this option shows a more stable model with a good mesh convergence analysis.

A force-displacement curve, shown in Fig... is generated from the first assumption, for this case

For both cases

## 5.7 Material model

In an ideal and first scenario, this material can be assumed as linear, isotropic, elastic and nearly incompressible. For this case, there are two main variables, the Young's Modulus  $E$ , and the Poisson's ratio  $\nu$ .

From the parametric analysis, it is possible to see that the bulk modulus of this material does not possess a big impact in the FE simulation results. This conclusion combined with the results from the Poisson ratio in the first material model coincide with the statements from Bergström, where it is not vital to know these parameters to obtain accurate FE computational models, as these have limited influence on the mechanical response. [2]



# 6 Conclusion and Outlook

## 6.1 Summary and Contributions

## 6.2 Recommendations for Future Research

## 6.3 Conclusions and Final Remarks



# A Frequently Asked Questions

## A.1 How do I change the colors of links?

The color of links can be changed to your liking using:

```
\hypersetup{urlcolor=red}, or  
\hypersetup{citecolor=green}, or  
\hypersetup{allcolor=blue}.
```

If you want to completely hide the links, you can use:

```
\hypersetup{allcolors= .}, or even better:  
\hypersetup{hidelinks}.
```

If you want to have obvious links in the PDF but not the printed text, use:

```
\hypersetup{colorlinks=false}.
```



# Bibliography

- [1] “Ansys Mechanical APDL Element Reference”. In: (Nov. 2010).
- [2] Jörgen Bergström. *Mechanics of Solid Polymers: Theory and Computational Modeling*. ISBN: 9780323311502.
- [3] Chen Ket Chai et al. “Local axial compressive mechanical properties of human carotid atherosclerotic plaques-characterisation by indentation test and inverse finite element analysis”. In: *Journal of Biomechanics* 46 (10 June 2013), pp. 1759–1766. DOI: 10.1016/j.jbiomech.2013.03.017.
- [4] Amirhossein Goharian, Seyed S.R. Koloor, and Mohamed R. Abdullah. *Biomechanical Evaluation Methods*. Elsevier Inc., Mar. 2017, pp. 65–87. DOI: 10.1016/B978-0-12-804634-0.00005-7.
- [5] Asif Husain, D. K. Sehgal, and R. K. Pandey. “An inverse finite element procedure for the determination of constitutive tensile behavior of materials using miniature specimen”. In: *Computational Materials Science* 31 (1-2 Sept. 2004), pp. 84–92. DOI: 10.1016/j.commatsci.2004.01.039.
- [6] J. Joseph et al. “Biomedical applications of polyurethane materials and coatings”. In: *Transactions of the Institute of Metal Finishing* (3 May 2018), pp. 121–129. DOI: 10.1080/00202967.2018.1450209.
- [7] Valentine Kanyanta and Alojz Ivankovic. “Mechanical characterisation of polyurethane elastomer for biomedical applications”. In: *Journal of the Mechanical Behavior of Biomedical Materials* 3 (Jan. 2010), pp. 51–62. ISSN: 17516161. DOI: 10.1016/j.jmbbm.2009.03.005.
- [8] M. Kauer et al. “Inverse finite element characterization of soft tissues”. In: *Medical Image Analysis* 6 (2002), pp. 275–287.
- [9] David C. Lin et al. “Spherical indentation of soft matter beyond the Hertzian regime: Numerical and experimental validation of hyperelastic models”. In: *Biomechanics and Modeling in Mechanobiology* (Oct. 2009), pp. 345–358. DOI: 10.1007/s10237-008-0139-9.
- [10] Kaifeng Liu, Mark R. VanLandingham, and Timothy C. Ovaert. “Mechanical characterization of soft viscoelastic gels via indentation and optimization-based inverse finite element analysis”. In: *Journal of the Mechanical Behavior of Biomedical Materials* 2 (Aug. 2009), pp. 355–363. DOI: 10.1016/j.jmbbm.2008.12.001.
- [11] Yuta Mori. “Development of a method for identifying the physical properties of post-extraction organs”. In: (Feb. 2022).
- [12] R.W. Ogden. *Non-Linear Elastic Deformations*. Dover Civil and Mechanical Engineering, Dover Publications, 2013. ISBN: 9780486318714.
- [13] Thomas J. Pence and Kun Gou. “On compressible versions of the incompressible neo-Hookean material”. In: *Mathematics and Mechanics of Solids* 20 (2 Feb. 2015), pp. 157–182. ISSN: 17413028. DOI: 10.1177/1081286514544258.

- 
- [14] Wenshou Wang and Chun Wang. *Polyurethane for biomedical applications: A review of recent developments*. Elsevier, 2012, pp. 115–151. DOI: 10.1533/9781908818188. 115.